Int. J. Environ. Sci. Technol. (2016) 13:1177–1188
DOI 10.1007/s13762-016-0952-0

ORIGINAL PAPER

Investigation on the effective remediation of quinoline at solid/solution interface using modified agricultural waste: an inclusive study

Md. J. K. Ahmed[1] · **M. Ahmaruzzaman**[1]

Received: 14 August 2015 / Revised: 23 December 2015 / Accepted: 8 February 2016 / Published online: 24 February 2016

Abstract This research work explores the potential of modified agricultural waste for the sorption of quinoline from aqueous media. A quinoline removal efficiency of around 97 % and sorption capacities of ~20 (batch) and ~35 mg g^{-1} (fixed-bed) were achieved. Pseudo-second-order kinetics and Temkin isotherm best represented the equilibrium sorption data. The sorption of quinoline is exothermic and spontaneous in nature with a slight increase in the system entropy. The quinoline sorption mechanism is controlled by H-bonding, π–π dispersive interactions, boundary layer, and intraparticle diffusion. Microwave–chemical integrated regeneration technique retrieves the sorption capacity of the exhausted sorbent with 99.15, 97.64, and 95.55 % of the original, in three sorption–regeneration cycles. Energy recovery (19.365 MJ kg^{-1}) from the quinoline-loaded sorbent and the potential utilization of left-over ash materials enhanced the prospective of the sorbent for the remediation of pollutants for a clean and green environment.

Keywords Fixed-bed · Intraparticle diffusion · Isotherm · Kinetics · Regeneration · Sorption

Introduction

Quinoline is a nitrogen-containing heterocyclic compound with a strong odour. It is widely present in petroleum refining and coal processing effluents, which amounts to worldwide production of greater than 2000 tonne per year (Collin and Hoke 1993). Besides, it is also present in pharmaceutical, pulp, and papermaking wastewater. It is generally used as raw material and solvent in the production of paints, dyes, herbicides, and chemicals (Jing et al. 2012). Environmental Protection Agency (EPA) has classified quinoline as a group B2 chemicals, probable human carcinogen. The perseverance and destiny of quinoline in wastewater need specific attention as it largely contributes to chemical oxygen demand (COD) in effluents. This creates a major obstacle in meeting the sewage discharge requirements on both COD (<50 mg L^{-1}) and NH_4-N (<5 mg L^{-1}) (Jing et al. 2014). Quinoline has greater water solubility than its homocyclic analogue due to the existence of a nitrogen atom in the aromatic ring system. Therefore, quinoline easily gets accumulated in industrial wastewaters and surface water and is a direct threat to ecosystems. It is well documented in the literature that quinoline is toxic, carcinogenic, mutagenic to animals and human being (Rameshraja et al. 2012). Thus, the removal of quinoline from aqueous media is a challenge to achieve for cleaner and healthier environment. Quinoline contaminated wastewater is treated by various physico-chemical (Enriquez and Pichat 2001; Jing et al. 2013) and biological processes (Bai et al. 2011). However, adsorption technology has been developed as a proficient and widespread method for wastewater treatment as per WHO and EPA guidelines (Ahmed and Ahmaruzzaman 2015a; Ali and Gupta 2007). A very limited number of researchers have reported the sorption of quinoline onto sorbents, such as silica gel (Moon et al. 1989), rundle spent shell (Zhu et al. 1988), kaolinite and montmorillonite (Burgos et al. 2002), unsaturated soil (Thomsen et al. 1999), granular activated carbon, and bagasse fly ash (Rameshraja et al. 2012). However, available literature does not have an inclusive study which covers diverse aspects of quinoline sorption, fixed-bed column studies, microwave–

✉ M. Ahmaruzzaman
md_a2002@rediffmail.com

[1] Department of Chemistry, National Institute of Technology Silchar, Silchar 788010, India

chemical regeneration, reusability of renewed sorbent, energy recovery, and disposal approaches of loaded sorbents. This motivates the authors to undertake a comprehensive study on the sorption of quinoline. The precursor for the sorbent under study is coconut coir, an agricultural waste, which is a hard endocarp material. It was chemically modified with H_3PO_4 treatment and used in authors' earlier research work for the sequestration of pyridine from aqueous solution and desulfurization of feed diesel (Ahmed et al. 2014; Ahmed and Ahmaruzzaman 2015c).

This research work investigates the quinoline sorption potential of chemically treated coconut coir waste in a wide concentration range of quinoline (50–400 mg L^{-1}). The sorption of quinoline was explored in batch system to optimize the operational parameters of sorption. Fixed-bed column studies were also performed. An integrated microwave–chemical regeneration was explored for the retrieval of sorption capacity of the exhausted sorbent, and the regenerated sorbents were reutilized for repetitive cycles. The recovery of energy and disposal approach of quinoline-loaded sorbent were also studied and reported. This research work was carried out on January 2015 at National Institute of Technology, Silchar.

Materials and methods

Materials

Analytical reagent (AR) grade chemicals were used in the present study without further purification. Ultrapure water (18.0 MΩ cm) from Merck Millipore Milli-Q system was used throughout the experiments. The target pollutant quinoline (chemical formula: C_9H_7N, formula weight: 129.16, purity: 98 %) was supplied by Alfa Aesar. A stock solution of 1000 mg L^{-1} quinoline was prepared by dissolving 0.468 mL quinoline in 500 mL ultrapure water under vigorous stirring for 2 min. The stock solution was diluted to requisite test concentration with ultrapure water. The sorbent used in this study was prepared by the chemical treatment of coconut coir waste as per procedure described elsewhere (Ahmed et al. 2014). Briefly, the precursor material was chemically impregnated with H_3PO_4 and carbonized in a muffle furnace at 723 K for 1 h. The carbonized product was repeatedly washed with ultrapure water, dried at 383 K for 6 h, pulverized, and referred to as modified agricultural waste (MAW).

Characterization of the sorbent

The sorbent (MAW) was characterized by proximate, CHN, yield of MAW and chemical recovery, carbon surface functionalities, thermogravimetric analysis (TGA), and Brunauer–Emmett–Teller (BET) surface area, pore size distribution (PSD), particle size, and Fourier transform infrared (FTIR) spectroscopy, scanning electron microscope (SEM) and X-ray diffraction (XRD) analyses. The surface functional group vibrations of the blank and quinoline-loaded MAW were recorded on a Thermo Nicolet (Nexus-870) FTIR spectrometer. SEM images of blank and quinoline-loaded MAW were observed on a CAMSCAN–2, JEOL scanning electron microscope.

Batch and fixed-bed sorption assay of quinoline

The sorption of quinoline was performed by the interaction of quinoline with MAW in aqueous media. The operational parameters of sorption such as solution pH (pH_o), sorbent load (m), and interaction time (t), initial concentration (C_o) and reaction temperature (T) were optimized. A quinoline concentration of 100 mg L^{-1} was used for all the batch experiments excluding isotherm study (C_o = 50–400 mg L^{-1}). The kinetic, isotherm, and thermodynamic studies for the sorption process were also performed. The experiments were carried out in stoppered Erlenmeyer flask kept in a temperature-controlled incubator cum shaker (shaking speed: 140 rpm). The test samples were withdrawn at the end of specified time, centrifuged, and the supernatant was analysed for residual quinoline concentration.

The transport of quinoline through fixed-bed system was also explored. The experimental set-up comprised a glass column of 30 cm bore length and 1.8 cm bore diameter, packed with 2.20 g MAW for a bed height of 1.82 cm. The fixed-bed column continuously transported an influent quinoline concentration of 100 mg L^{-1} at a constant flow rate of 1.0 mL min^{-1} under the influence of gravity. The effluents were tested for quinoline at various times, and the column run was stopped when the effluent concentration was same as the influent concentration.

Regeneration of exhausted sorbent and its reusability

After the sorption of quinoline, the exhausted MAW was exposed to microwave (MW) irradiation for the retrieval of its sorption capacity. The quinoline-loaded MAW was dried at 383 K for 1 h in a hot air oven and then interacted with 1N HNO_3 for 15 min. The resulting mixture was MW irradiated (2.45 GHz, 360 W) for 5 min. The MW-treated material was thereafter subjected to washings with ultrapure water till pH ~7, and this completes the regeneration process. The quinoline-loaded MAW was also exposed to increasing MW irradiation (540, 720, and 900 W), and the subsequent effects on the sorption capacity were also examined. The regenerated MAW was reutilized for the sorption of quinoline, and the sorption–regeneration was run for three cycles.

Analytical measurement of quinoline

The residual concentration of quinoline in the supernatant after sorption and regeneration was analysed by a Thermo Scientific UV–Visible spectrophotometer at λ_{max} of 276 nm. The removal percentage and sorptive uptake of quinoline were estimated with mass-balance equations (Ahmed and Ahmaruzzaman 2015b):

$$\text{Removal percentage of quinoline} = \frac{(C_o - C_e)}{C_o} \times 100 \quad (1)$$

$$\text{Sorptive uptake of quinoline per } g \text{ of MAW; } q_e = \frac{(C_o - C_e) \times V}{m} \quad (2)$$

where C_o and C_e are initial and equilibrium concentrations (mg L^{-1}) of quinoline, V is the volume (L) of test sample, and m is the weight (g) of MAW.

Results and discussion

Characterization of MAW

The carbon, hydrogen, and nitrogen content of the MAW were determined as 55.53, 3.28, and 0.98 wt%, respectively. TGA studies revealed thermal degradation at around 450–600 °C, the maximum degradation at around 650 °C. The sorbent has a particle size of 33.35 μm with a BET surface area of ~1255 m^2 g^{-1} and adsorption pore volume of 1.02 cm^3 g^{-1}, which indicates favourable sorption of quinoline. The details of the characterization results were explained elsewhere (Ahmed et al. 2014).

The quinoline-loaded MAW was analysed with FTIR and SEM investigations to justify the sorption of quinoline. The surface functional groups of MAW were investigated by Fourier transform infrared (FTIR) spectroscopy. Figure 1a, b shows the FTIR spectra of blank and quinoline-loaded MAW. The absorption bands for blank MAW at 3438, 1729, 1035 cm^{-1}, around 1400, and 1600 cm^{-1} correspond to H-bonded OH stretch, C=O stretching of carboxylic acid, C–N stretch of primary amine, bounded water coordinated with cations, and hydrogen bonding vibrations, respectively (Ahmed and Ahmaruzzaman 2015d). The absorption bands at 3438, 1729, and 1035 cm^{-1} shift to 3360, 1720, and 1043 cm^{-1}, respectively, which illustrates the involvement of these functional groups in the sorption of quinoline. The slight shifting of absorption bands at around 1400 and 1600 cm^{-1} also suggests their role in the sorption of quinoline. The SEM images of the sorbent help in the better understanding of the surface morphology. Figure 2a shows the SEM image of blank MAW. The observed image shows high roughness on the sorbent surface with haphazardly oriented pits. These provide larger effective surface for the easy sorption of quinoline molecules. The surface roughness of the

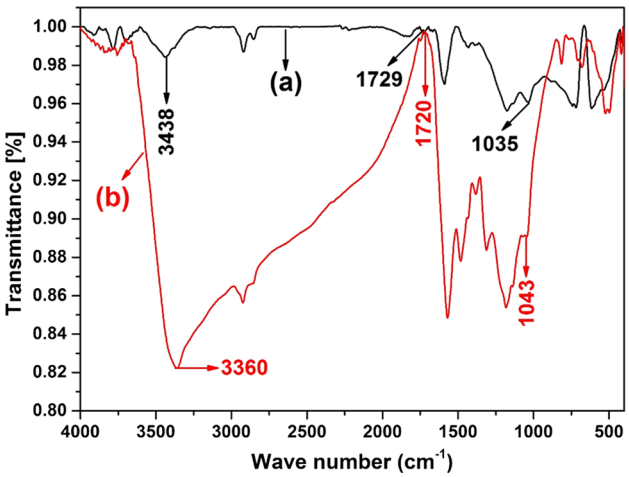

Fig. 1 FTIR spectra of (*a*) blank and (*b*) quinoline-loaded MAW

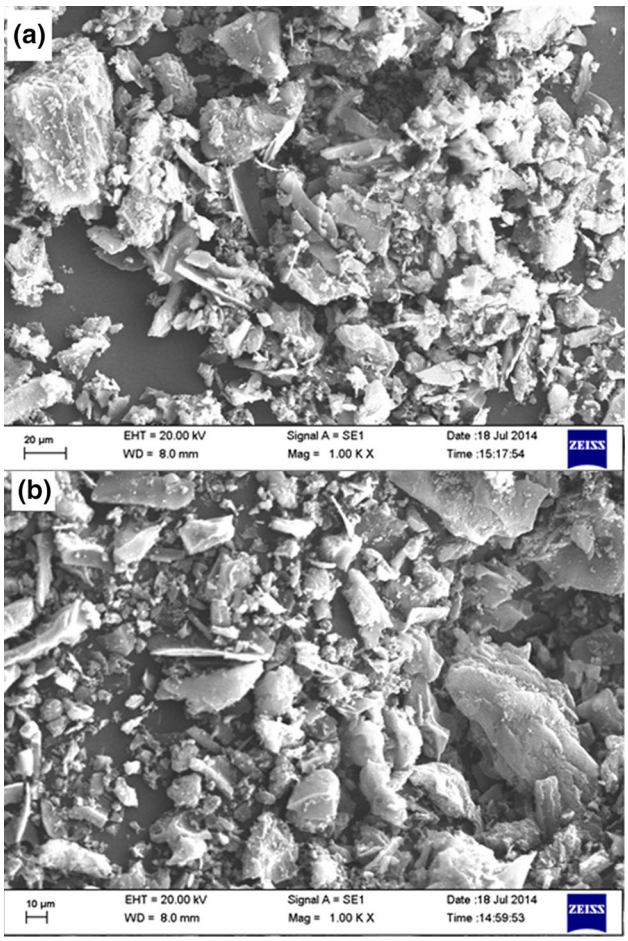

Fig. 2 SEM images of **a** blank and **b** quinoline-loaded MAW

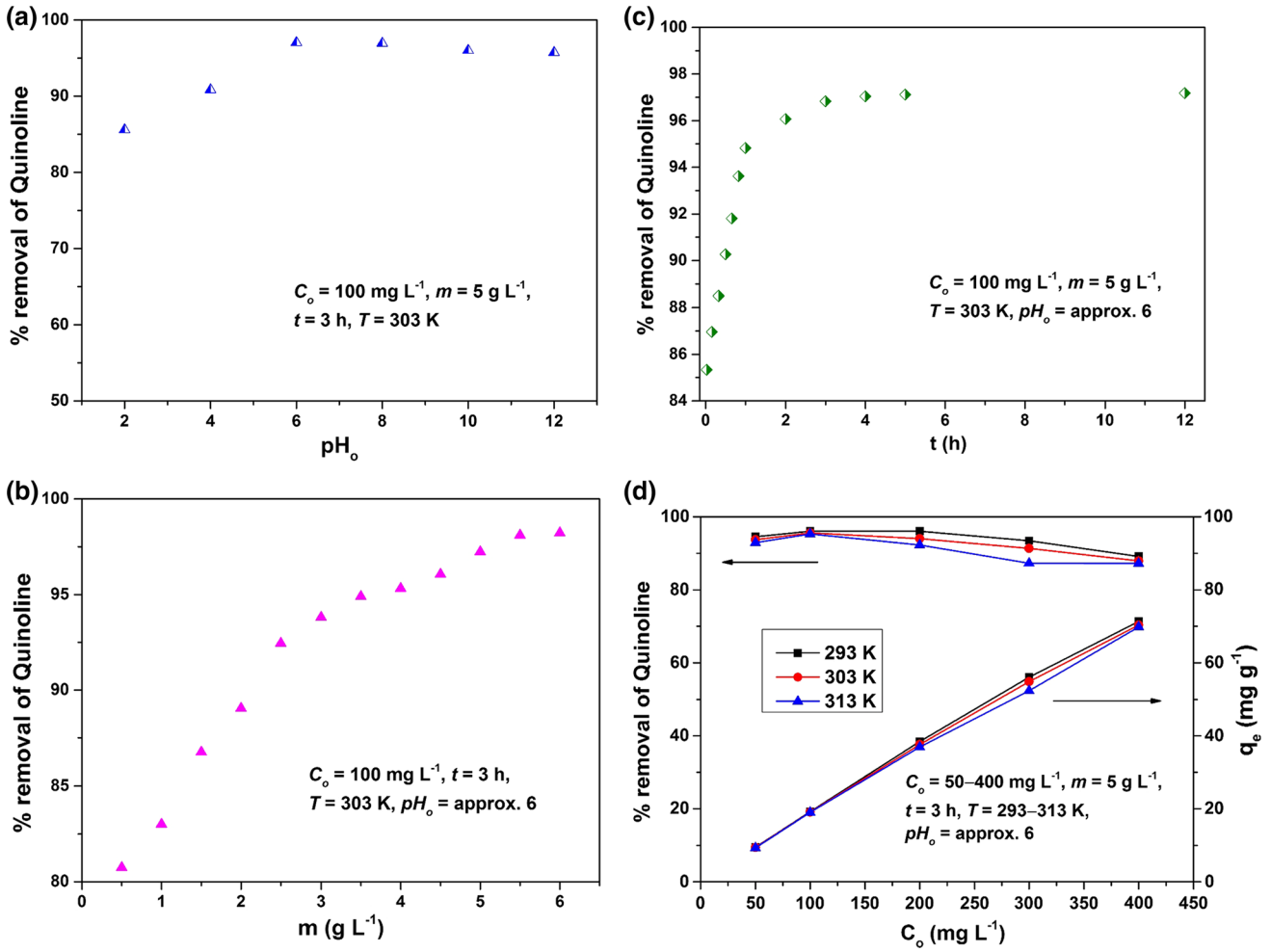

Fig. 3 Influence of operational parameters on quinoline sorption **a** initial pH (pH_o), **b** sorbent load (m), **c** interaction time (t), and **d** initial concentrations (C_o) at different temperatures (T)

sorbent and development of pits may be resulted from the chemical treatment of the agricultural waste. A decrease in the surface roughness (faintly observed) in the SEM image of quinoline-loaded MAW is shown in Fig. 2b. This may be considered as an indication of the adherence of quinoline molecules on the sorbent surface.

Batch sorption of quinoline at solid/solution interface

The sorption of quinoline was investigated in batch system to optimize operational parameters, and their subsequent effects on the uptake of quinoline were also studied. The sorption of quinoline as a function of increasing solution pH (C_o = 100 mg L^{-1}, m = 5 g L^{-1}, t = 3 h, T = 303 K) is shown in Fig. 3a. The per cent removal of quinoline increases with the increase in solution pH from 2–6, but does not change significantly from 6–12. This increasing trend may be due to the decrease in H^+ ion concentration with increasing pH unlike lower pH, where H^+ ion competes with the sorption of quinoline. The natural pH of quinoline is around 6, and it is observed that maximum per cent removal is achieved at natural pH.

The influence of increasing sorbent load (m) on the sorption of quinoline (C_o = 100 mg L^{-1}, t = 3 h, T = 303 K, pH_o = ~6) is shown in Fig. 3b. It is observed that with the increase in sorbent load from 0.5–5 g L^{-1}, the per cent removal of quinoline increases from 80.74 to 97.24 %. This increasing trend of quinoline sorption is due to the higher accessibility of effective surface area and active surface functional groups (Santhi et al. 2009). A further increase in m from 5–6 g L^{-1} increased the sorption of quinoline by marginal amount of 0.98 %. This may be due to the attainment of equilibrium and overcrowding of quinoline molecules at the active sites of MAW. Thus, the optimum value of m for quinoline sorption is 5 g L^{-1}. It is worth mentioning that a high per cent removal of quinoline (80.74 %) is achieved even with lower sorbent load of 0.5 g L^{-1}, which signifies the high effectiveness of MAW.

The effect of increasing interaction time on the sorption of quinoline ($C_o = 100$ mg L^{-1}, $m = 5$ g L^{-1}, $T = 303$ K, $pH_o = \sim 6$) is shown in Fig. 3c. At initial state of sorption (2 min), 85.34 per cent removal is achieved with gradual increase to 96.83 % at the end of 3 h. After that, the attainment of saturation state is designated with a plateau line till 12 h. At the initial stage of interaction time, a quick uptake of quinoline is observed maybe due to concentration gradient between quinoline concentration in the bulk of the solution and on the surface of MAW. A quasi-equilibrium is reached at the end of 3 h as a marginal increase (0.36 %) in quinoline sorption is achieved from 3–12 h. Hence, 3 h is considered as the optimum interaction time for the sorption of quinoline.

The per cent removal and sorption capacity of MAW as a function of initial quinoline concentration ($C_o = 50$–400 mg L^{-1}) at different reaction temperatures ($T = 293$–313 K) ($m = 5$ g L^{-1}, $t = 3$ h, $pH_o = \sim 6$) are shown in Fig. 3d. The removal efficiency of quinoline is 93.74 % at lower C_o (50 mg L^{-1}). With increasing initial quinoline concentration, a decrease in the per cent removal is observed. The decreasing trend of per cent removal at higher C_o may be due to the greater extent of competing quinoline molecules in the aqueous media with lesser accessibility to the active sites of the sorbent. However, MAW proved to be an effective sorbent for the uptake of quinoline even at higher C_o (400 mg L^{-1}) with 87.94 % sorption efficiency at 303 K. Contrary to the above discussion, a rapid uptake of quinoline is observed with increasing C_o. This can be due to the fact that at higher C_o a greater mass driving force is anticipated by the quinoline molecules. As reaction temperature increases from 293 to 313 K, the sorption efficiency (for $C_o = 100$ - mg L^{-1}) decreases from 96.07 to 95.28 %. It indicates the exothermic nature of quinoline sorption onto MAW.

Investigation of sorption kinetics

The kinetic investigation of quinoline sorption gives an idea about the equilibrium interaction time and mass transfer of quinoline molecules. The equilibrium sorption data at different time intervals are examined by various kinetic models, such as (Ahmaruzzaman et al. 2015):

$$\text{Lagergren Pseudo-first order equation: } \log(q_e - q_t) = \log q_e - \left(\frac{k_1}{2.303}\right)t \quad (3)$$

$$\text{Ho and McKay Pseudo-second order equation: } \frac{t}{q_t} = \frac{1}{k_2 q_e^2} + \left(\frac{1}{q_e}\right)t \quad (4)$$

$$\text{Webber-Morris Intraparticle diffusion: } q_t = k_{ip}t^{1/2} + C \quad (5)$$

where q_e and q_t (mg g^{-1}) are sorption capacities at equilibrium and at time 't', respectively; k_1 (h^{-1}) is the pseudo-first-order rate constant and k_2 (g mg^{-1} h^{-1}) is the pseudo-second-order rate constant. k_{ip} is the intraparticle diffusion rate constant, and values of C give an idea about thickness of the boundary layer.

The various kinetic models are validated by the normalized standard deviation (Δq %) given by:

$$\Delta q(\%) = 100\sqrt{\frac{\sum\left[\frac{(q_{exp} - q_{cal})}{q_{exp}}\right]^2}{(N-1)}} \quad (6)$$

where q_{exp} and q_{cal} (mg g^{-1}) are the experimental and calculated sorption capacities, respectively. N is the number of data points in the graph, which corresponds to the kinetic equation.

The kinetic plots for pseudo-first-order, pseudo-second-order, intraparticle diffusion, and mass transfer models are shown in Fig. 4. The kinetic parameters for different kinetic models are given in Table 1. Pseudo-second-order kinetic model best fits the equilibrium data with better correlation coefficient ($R^2 = 0.999$) and least normalized standard deviation ($\Delta q\% = 0.039$). Moreover, the calculated q_e value is closer to the experimental q_e value. A significant boundary layer effect is also observed from the calculated C values.

Sorption isotherm

The equilibrium data are fitted to Langmuir (Langmuir 1916), Freundlich (Freundlich 1906) and Temkin isotherms (Temkin and Pyzhev 1940) to ascertain the best model that validates the sorption of quinoline. The corresponding isotherm equations are given below.

$$\text{Langmuir isotherm: } \frac{C_e}{q_e} = \frac{1}{a_L b_L} + \frac{C_e}{a_L} \quad (7)$$

$$\text{Freundlich isotherm: } \log q_e = \log K_F + \frac{1}{n}\log C_e \quad (8)$$

$$\text{Temkin isotherm: } q_e = \left(\frac{RT}{b_T}\right)\ln K_T + \left(\frac{RT}{b_T}\right)\ln C_e \quad (9)$$

where C_e (mg L^{-1}) is the equilibrium concentration of the adsorbate, q_e (mg g^{-1}) is the adsorptive uptake per unit weight of the adsorbent, and a_L (mg g^{-1}) and b_L (L g^{-1}) are Langmuir constant related to monolayer adsorption capacity and energy of adsorption, respectively. K_F (L mg^{-1}) and $1/n$ are the Freundlich adsorption constant and a measure of adsorption efficiency, respectively. R (8.314 J K^{-1} mol^{-1}) is the universal gas constant, T (K) is the absolute temperature, and b_T and K_T are the constant related to heat of adsorption and equilibrium binding constant corresponding to maximum binding energy, respectively.

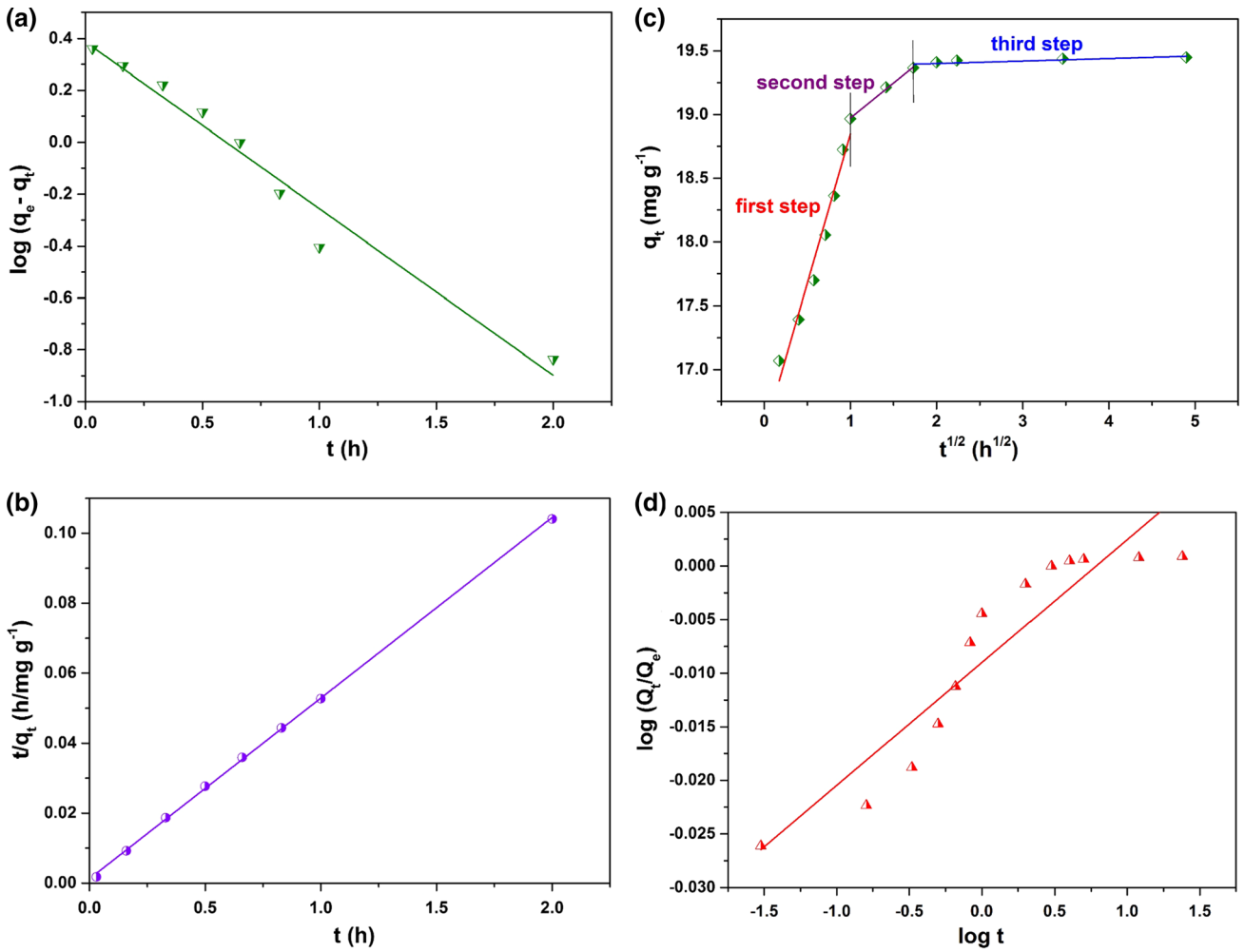

Fig. 4 **a** Pseudo-first-order, **b** pseudo-second-order, **c** intraparticle diffusion, and **d** mass transfer kinetics of quinoline sorption onto MAW; $C_o = 100$ mg L^{-1}, $T = 303$ K, $m = 5$ g L^{-1}

Table 1 Kinetic parameters for the sorption of quinoline onto MAW; $C_o = 100$ mg L^{-1}, $T = 303$ K, $m = 5$ g L^{-1}

Model	Parameters	Units	Values		
Pseudo-first-order	$q_{e,\,exp}$	mg g^{-1}	19.36		
	$q_{e,\,cal}$	mg g^{-1}	2.43		
	k_1	h^{-1}	1.47		
	R^2		0.965		
	Δq	%	33.05		
Pseudo-second-order	$q_{e,\,cal}$	mg g^{-1}	19.38		
	k_2	g mg^{-1} h^{-1}	2.164		
	R^2		0.999		
	Δq	%	0.039		
			First step	Second step	Third step
Intraparticle diffusion	k_{ip}	mg g^{-1} $h^{1/2}$	2.34	0.549	0.53
	C	mg g^{-1}	16.51	18.42	98.03
	R^2		0.965	0.992	0.523

The linearized data fitting for Langmuir, Freundlich, and Temkin isotherms at various temperatures, experimental isotherm plot, and its validity at 303 K are shown in Fig. 5. The isotherm parameters for various models and their corresponding correlation coefficient (R^2) at different temperatures are given in Table 2. Figure 5a shows the

Langmuir isotherm for the sorption of quinoline. The feasibility and vital characteristics of Langmuir isotherm are ascertained with dimensionless separation factor (R_L), given by the following equation (Ahmed et al. 2015):

$$R_L = \frac{1}{1 + b_L C_o} \tag{10}$$

The sequestration process is favourable when $0 < R_L < 1$, unfavourable ($R_L > 1$), linear ($R_L = 1$), and irreversible ($R_L = 0$). R_L values less than unity at various temperatures validate the feasibility of the Langmuir isotherm. The assessment of Freundlich isotherm (Fig. 5b) parameters shows substantial K_F values with $1/n$ values lower than unity at different temperatures. This indicates favourable sorption as $1/n < 1$. The decreasing K_F values with increasing temperature signify the exothermic nature of quinoline sorption. In the case of Temkin isotherm (Fig. 5c), the equilibrium data behaved almost linearly with significantly high R^2 values and heat of adsorption (b_T) for various temperatures. On the basis of correlation coefficient (R^2) closest to unity for the three isotherms at different temperatures, the fitting is Temkin < Langmuir < Freundlich.

Figure 5d shows the experimental isotherm plot for the sorption of quinoline at different temperatures. The profile resembles type II isotherm (classified by IUPAC) for macroporous materials with strong interaction between the sorbent and quinoline molecules. The validity of the three isotherm models with respect to the experimental isotherm is shown in Fig. 5e. Figure shows that Temkin isotherm profile is closest to the experimental data with lesser deviation than Freundlich and Langmuir isotherms.

Thermodynamics of quinoline sorption

The thermodynamic parameters of quinoline sorption onto MAW are calculated using the following thermodynamic equations (Ahmaruzzaman et al. 2015):

$$K_c = \frac{C_s}{C_e} \tag{11}$$

$$\Delta G^o = \Delta H^o - T\Delta S^o \tag{12}$$

$$\ln K_{ad} = -\frac{\Delta H^o}{RT} + \frac{\Delta S^o}{R} \tag{13}$$

where K_c is equilibrium constant and C_s and C_e (mg L^{-1}) are equilibrium concentrations of quinoline in solid and liquid phase, respectively. ΔG^o (kJ mol^{-1}), ΔH^o (kJ mol^{-1}), and ΔS^o (J mol^{-1} K^{-1}) represent the change in Gibb's free energy, enthalpy, and entropy of the system, respectively. T (K) is the reaction temperature in absolute scale, and R (8.314 J mol^{-1} K^{-1}) is the universal gas constant.

The change in enthalpy and entropy of the system is calculated from the slope and intercept of van't Hoff plot ($\ln K_c$ vs. $1/T$, plot not shown), respectively. The corresponding values for free energy change at various temperatures are estimated from Eq. (12). The negative value of ΔH^o (−7.32 kJ mol^{-1}) confirms the exothermic nature of sorption. A slight increase in the randomness of the reaction system is established from the positive value of ΔS^o (1.52 J K^{-1} mol^{-1}). This might be due to the displacement of adsorbed water molecules on the sorbent surface by quinoline resulting into transitional entropy gain than lost by quinoline molecules (Baccar et al. 2013). The negative values of ΔG^o, −7.76, −7.78, and −7.79 kJ mol^{-1} at 293, 303, and 313 K, respectively, confirm the feasibility and spontaneity of the sorption process. A decrease in ΔG^o with increasing reaction temperature signifies lesser driving force, which results into lower sorption capacity at higher temperatures.

Mechanism of quinoline interaction with the sorbent

The insight into the sorption mechanism of quinoline onto MAW helps in better understanding of the uptake phenomena. It is inferred from the FTIR analysis that the following surface functional groups such as OH stretching of the hydroxyl group, C=O stretching of carboxylic acid, and adsorbed water bounded onto the sorbent surface interact with quinoline for the sorption to take place. The shifting of the absorption bands of these functional groups after the loading of quinoline confirms the sorption phenomena.

The understanding of the sorption mechanism reveals the involvement of π–π dispersive interaction between the π-electrons of the aromatic ring of quinoline and that of graphene layer of MAW. Quinoline is a π-electron containing hetero-aromatic compound and with increasing pH; its π-electron density increases facilitating easy interaction with the π-electrons of the graphene layer of MAW (Alonso-Davilla et al. 2012). This is in accordance with the increasing sorption efficiency with increasing pH from 2–6.

The sorption of quinoline may be governed by single, many or by a combination of steps: boundary layer or film or external diffusion, pore diffusion, surface diffusion, and sorption on pores. Weber–Morris plot (q_t vs. $t^{1/2}$) explains the controlling mechanism of quinoline sorption (Weber and Morris 1962). A linear Weber–Morris plot with zero intercept signifies intraparticle diffusion as the sole rate controlling step. However, in the sorption of quinoline a number of diffusion mechanisms got involved. Weber–Morris plot shown in Fig. 4c shows the participation of three steps in the sorption of quinoline. The first step implies boundary layer diffusion; the second designates mesoporous intraparticle diffusion and the third microporous intraparticle diffusion. Thus, the sorption of

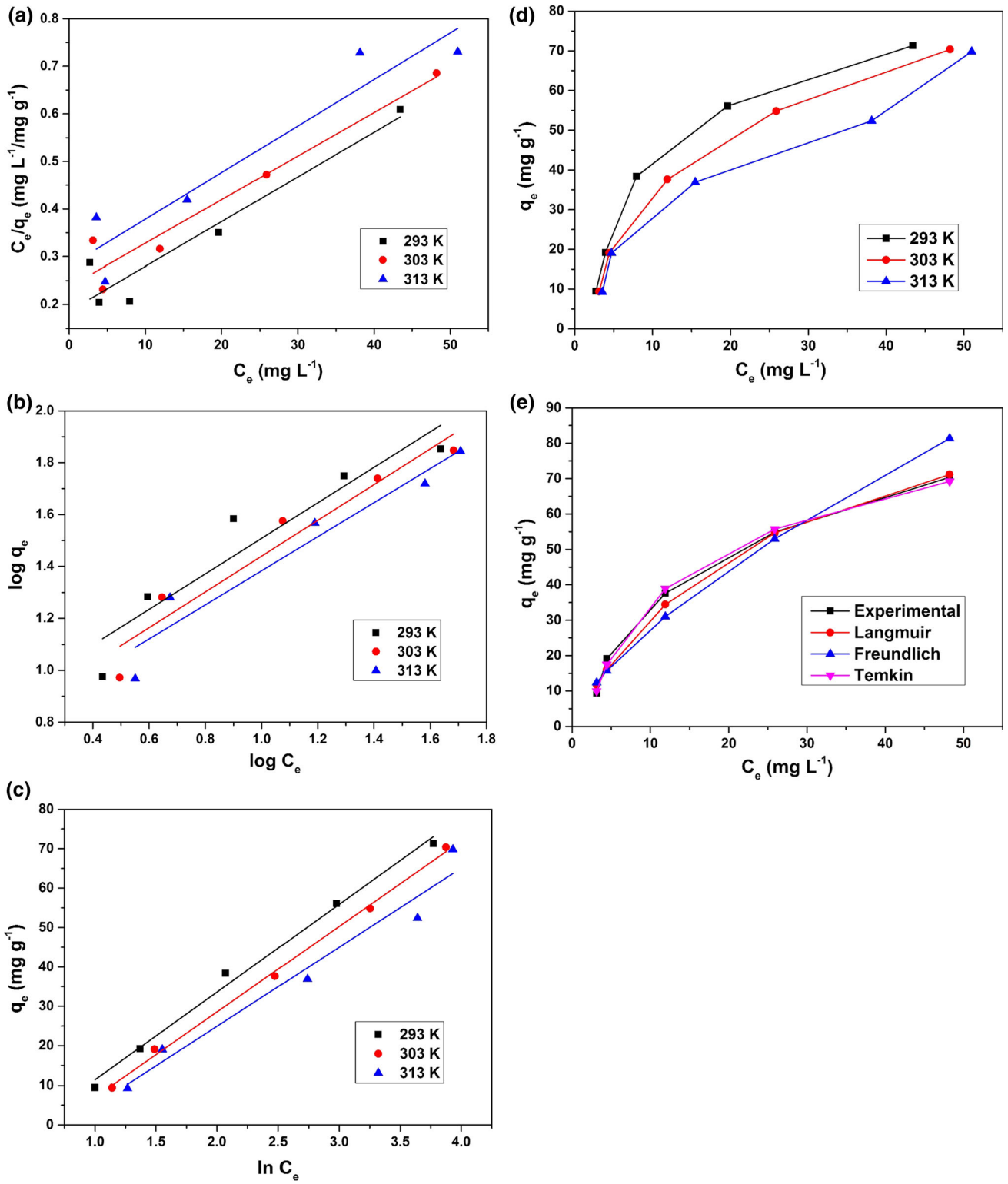

Fig. 5 **a** Langmuir, **b** Freundlich, **c** Temkin, **d** C_e versus q_e plot, and **e** validity of different isotherms (at 303 K) for the sorption of quinoline onto MAW at various temperatures

quinoline takes place via a complex mechanism. The sorption of quinoline at the initial phase (via boundary layer diffusion) is the fastest step due to greater accessibility of active sites of the sorbent. The third step with microporous intraparticle diffusion is the rate-limiting step in the sorption process. The pore diffusion constant

Table 2 Isotherm parameters for the sorption of quinoline onto MAW

Temp. (K)	a_L (mg g^{-1})	b_L (L g^{-1})	R_L	R^2
Langmuir isotherm				
293	106.61	0.0504	0.1656	0.88
303	109.41	0.0386	0.2057	0.92
313	102.25	0.0348	0.2232	0.87
Temp. (K)	$1/n_F$	K_F (L mg^{-1})		R^2
Freundlich isotherm				
293	0.684	6.67		0.86
303	0.689	5.64		0.91
313	0.656	5.53		0.91
Temp. (K)	b_T	K_T (L mg^{-1})		R^2
Temkin isotherm				
293	109.44	0.6124		0.99
303	116.19	0.5054		0.99
313	129.69	0.4686		0.95

(D, cm^2 s^{-1}) for quinoline sorption is given by Eq. (14) (Helfferich 1963).

$$t^{1/2} = \frac{0.03r^2}{D} \tag{14}$$

where $t^{1/2}$ is the half of the equilibrium interaction time (s) and r_o is the diameter of the sorbent (33.35×10^{-4} cm). The calculated value of D (6.179×10^{-11} cm^2 s^{-1}) infers insignificant pore diffusion. The mode of diffusion is determined from the transport number (n) using Eq. (15) (Kim et al. 1993).

$$\log Q_t/Q_e = \log k + n \log t \tag{15}$$

where Q_t and Q_e are weight of quinoline-loaded MAW at time t and at equilibrium. k is the quinoline–sorbent interaction coefficient. The value of n infers the type of transport mechanism. A value of $n \leq 0.5$ signifies Fickian transport, and $n \geq 1$ shows non-Fickian transport mechanism. A plot of log Q_t/Q_e versus log t is shown in Fig. 4d. The slope and intercept of the plot give the value of n (0.01) and k (0.98), respectively. Thus, Fickian transport mechanism controls the diffusion of quinoline into the pores of the sorbent.

Evaluation of sorption capacity in fixed-bed assay

To evaluate the full-scale industrial application of the sorbent, the sorption of quinoline in fixed-bed continuous assay is also explored. The breakthrough curve for the sorption of quinoline in fixed-bed mode is shown in Fig. 6. The fixed-bed column parameters were calculated with the help of the following equations (Gupta et al. 2011):

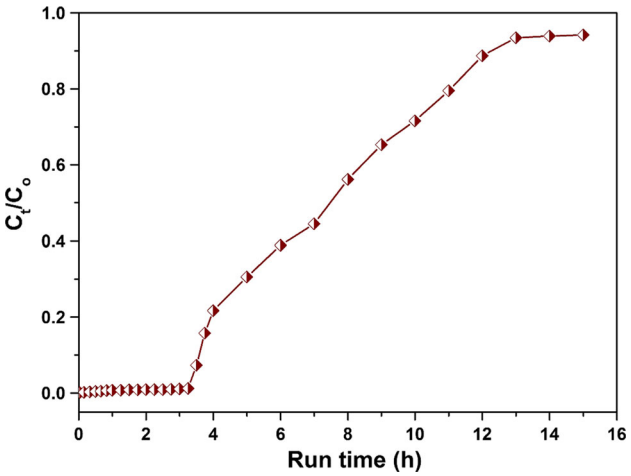

Fig. 6 Breakthrough curve for quinoline sorption onto MAW in fixed-bed system; $C_o = 100$ mg L^{-1}, $F = 1.0$ mL min^{-1}, $m = 2.20$ g, bed height = 1.82 cm

$$q_{\text{tot}}(\text{mg}) = \frac{t_s \times F \times (C_o - C_b)}{1000} \tag{16}$$

$$q_b(\text{mg}) = \frac{t_b \times F \times (C_o - C_s)}{1000} \tag{17}$$

$$M_{\text{tot}}(\text{mg}) = \frac{t_s \times F \times (C_o)}{1000} \tag{18}$$

$$\%\text{RM} = \frac{q_{\text{tot}}}{M_{\text{tot}}} \times 100 \tag{19}$$

$$q_e\left(\text{mg g}^{-1}\right) = \frac{q_{\text{tot}}}{m} \tag{20}$$

where C_s and C_b are quinoline concentration (mg L^{-1}), q_{tot} and q_b are amount of quinoline (mg) retained by the sorbent, and t_s and t_b are time (min), at saturation and breakthrough point, respectively. F is the flow rate (mL min^{-1}), M_{tot} is the total quinoline solution supplied, RM is the rate of quinoline removal by the column, q_e is the sorption capacity (mg g^{-1}), and m is the mass (g) of the sorbent. The fixed-bed study revealed a breakthrough time of 3.25 h and saturation time of 13 h. The calculated values for q_{tot}, q_b, M_{tot}, % RM, and q_e are 77.06 mg, 1.26 mg, 78.0 mg, 98.8 %, and 35.03 mg g^{-1}, respectively. Hence, it can be inferred that the sorbent has great potential in the uptake of quinoline for industrial use.

Comparative assessment of sorption capacity of MAW in batch and fixed-bed assay

The quinoline sorption capacity of MAW is ~20 and ~35 mg g^{-1} in batch and fixed-bed system, respectively. The percentage removal of quinoline is ~97 % in batch and around 99 % in fixed-bed column mode. The observed trend of increasing percentage removal and sorption capacity in fixed-bed assay may be attributed to the

continuous contact of MAW with almost constant quinoline concentration at sorbent/quinoline interface. This led to an increasing mass driving force and hence boost the sorption capacity of MAW. Contrary to the above fact, there is a decreasing mass driving force in batch system due to constant lowering of quinoline concentration as the sorption proceeds towards equilibrium. Consequently, a lower sorption capacity of MAW is encountered.

Retrieval of sorption efficiency of exhausted MAW by integrated microwave–chemical regeneration and its reusability studies

The regeneration performance of quinoline-loaded MAW was investigated by integrated MW–chemical approach due to increasing concern for waste minimization, retrieval of sorption efficiency, and industrial use. Quinoline-loaded sorbent was regenerated as per procedure described in Materials and Methods section. Due to MW irradiation, the quinoline molecules come to the surface of the sorbent and get extracted by nitric acid, which results in the removal of quinoline from the sorbent. Unlike conventional heating by convection where gases at high temperature deport from the surface to the centre of material, MW heats the material from the inner core developing a decreasing temperature gradient towards the surface (Liao et al. 2013). Hence, an easy transport of the desorbed molecules from core region at higher temperature to surface at lower temperature takes place. This, in turn, results in better conservation of textural characteristics of the material by reducing coke deposits in the porous domain. However, in case of convection heating, decomposition of desorbed molecules occurs resulting into rupture of pore walls and eventual loss of textural properties of the material (Ania et al. 2005).

The regenerated sorbent (MW irradiation: 360 W) was further explored for three sorption–regeneration cycles under similar experimental conditions. Figure 7a shows the sorption efficiency of regenerated MAW for three sorption–regeneration cycles. The renewed material shows quinoline sorption efficiency of 96.18, 94.71, and 92.68 % in three runs in comparison to 96.83 % for virgin MAW, which shows that the quinoline-loaded sorbents were regenerated almost completely. Therefore, it has been observed that 99.15, 97.64, and 95.55 % of the sorption capacity of virgin MAW were retained by the regenerated sorbent in three successive runs, respectively. However, a decrease in the sorption capacity of the regenerated sorbent with increasing MW irradiation is observed. Figure 7b shows the effect of MW irradiation on the quinoline sorption capacity of regenerated MAW. As MW irradiation increases from 360 to 900 W, the sorption efficiency decreases from 96.18 to 90.26 %. This can be due to partial decomposition of quinoline molecules at higher irradiation resulting into coke deposits and pore blockage. Moreover, rupture of pore walls may also takes place reducing the effective surface area of the sorbent (Liao et al. 2013).

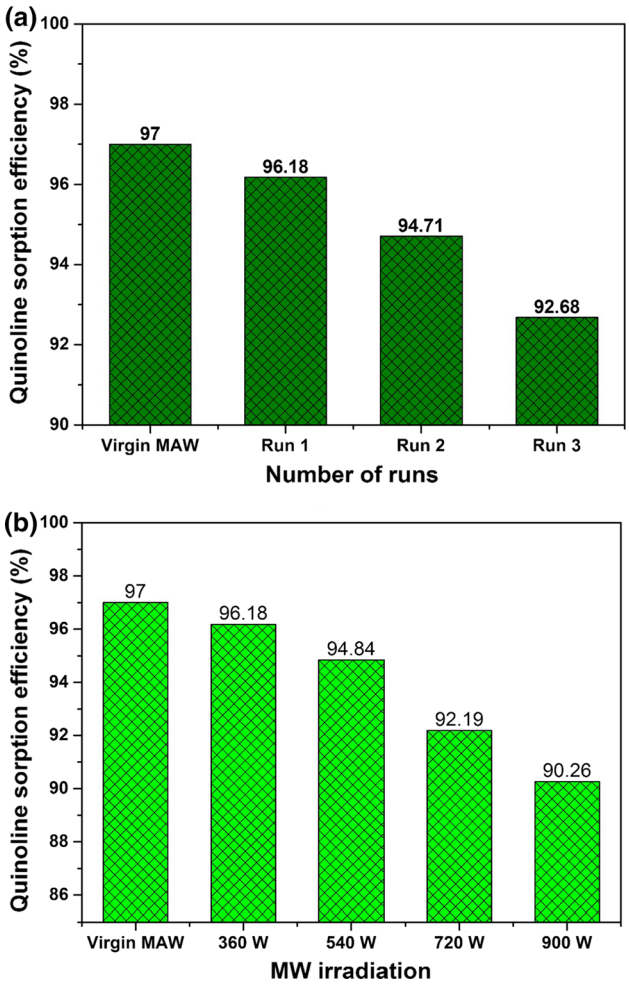

Fig. 7 Sorption efficiency of regenerated MAW **a** for three sorption–regeneration cycles and **b** effect of increasing MW irradiation

Energy recovery and disposal approaches of exhausted sorbent

On the complete loss of quinoline sorption capacity of MAW after repeated sorption–regeneration cycles, it was further utilized to recover energy. This is a significant step towards the comprehensive exploitation of the sorbent. The recovery of energy in terms of higher heating value (HHV) for quinoline-loaded MAW is around 19.365 MJ Kg^{-1}. This signifies the potential utilization of exhausted sorbent in the fabrication of fuel cakes for usage in furnaces and incinerators. Subsequently, the left-over bottom-ash materials may be utilized for the replacement of cement to a proportion where no loss in compressive strength of the building block is encountered. Hence, the possibility of

Table 3 Comparative data of quinoline sorption on various sorbents

Sorbents	Sorbent load (g L^{-1}) for C_o = 100 mg L^{-1}	Initial Conc. (mg L^{-1})	Equil. time (h)	Removal efficiency (%)	Sorption capacity (mg g^{-1})	References
Granular activated carbon (GAC)	10	50–1000	4–10	~85	8.78–77.82	Rameshraja et al. (2012)
Bagasse fly ash (BFA)	30	50–1000	4–10	~80	5.07–32.67	Rameshraja et al. (2012)
Silica gel	–	–	–	–	0.7581	Moon et al. (1989)
Modified agricultural waste (MAW)	5	50–400	3	~97	~9.5–72	This work

secondary pollution by quinoline-loaded MAW may be ruled out in a better way for a cleaner environment.

Comparative studies on sorption of quinoline onto MAW with other sorbents

cA comparative data analysis for sorption capacities of various sorbents with MAW and other aspects of sorption phenomena has been accomplished. Table 3 shows the quinoline sorption onto various sorbents under a wide range of operational parameters. The sorbent under study possess highest removal efficiency of around 97 % and sorption capacity of ~9.5–72 mg g^{-1} for C_o = 50–400 mg L^{-1}. Rameshraja et al. studied the sorption of quinoline for C_o (50–1000 mg L^{-1}) with ~80 % removal (BFA) and ~85 % removal (GAC). However, MAW shows a removal of ~97 % in the concentration range of 50–400 mg L^{-1}. The sorption capacities of GAC are 8.78, 18.97, and 77.82 mg g^{-1} for C_o = 50, 100, and 1000 mg L^{-1}, respectively. In the case of BFA, the sorption capacities are 5.07, 9.15, and 32.67 mg g^{-1} for C_o = 50, 100, and 1000 mg L^{-1}, respectively. In the present study, MAW shows sorption capacities of ~9.5, 20, and 72 mg g^{-1} for C_o = 50, 100 and 400 mg L^{-1}, respectively. In this regard, it is noteworthy to highlight that as concentration increases sorption capacity increases due to greater mass driving force of adsorbate. Unlike other sorption studies, the present sorption phenomena reach quick equilibrium at 3 h. Sorption efficiencies of 80.74 % (m = 0.5 g L^{-1}) and 97.24 % (m = 5 g L^{-1}) are achieved at low C_o (100 mg L^{-1}), whereas 87.94 % (m = 5 g L^{-1}) is attained at high C_o (400 mg L^{-1}). Other researchers (Moon et al. 1989; Zhu et al. 1988) also studied the sorption of quinoline but did not cover the fixed-bed sorption studies, efficient MW–chemical integrated regeneration, retrieval of sorption capacity of renewed sorbent without significant loss, recovery of energy from exhausted quinoline-loaded sorbent and potential disposal approaches of quinoline-loaded sorbent. Hence, the present research work is an inclusive study covering wide aspects for the sorption of quinoline from aqueous solutions.

Inferences suggesting real-world usage

Investigation on the sorption phenomena inferred the real-world application of MAW for the sorption of quinoline. This research work highlights MAW as a renewable sorbent with high percentage removal and sorption capacity for quinoline in aqueous media. All the characterization results demonstrate the good candidature of MAW for the uptake of quinoline and similar nitrogen heterocyclic compounds. Moreover, the low cost of MAW (US $ 10.714 per kg) in comparison with high-cost commercial activated carbon (US $ 172.96 per kg) proves the former as a good alternative to the latter in view of economic consideration. The ease of regeneration without significant loss in sorption capacity validates the real-world application of the sorbent. The recovery of energy from exhausted sorbent after repeated regeneration–sorption cycles and potential applications of left-over ash materials confirm the industrial viability of the sorbent.

Conclusion

MAW has been proved to be a low-cost, renewable, and highly efficient material for the sorption of quinoline from aqueous media. The sorption process achieves equilibrium at 3 h with a load of 5 g L^{-1} for natural pH (~6). It exhibits high sorption efficiency of around 97 % in batch and 99 % in fixed-bed assay. The sorption capacity of MAW is around 20 and 35 mg g^{-1} in batch and column system, respectively. Pseudo-second-order kinetics and Temkin isotherm well represent the equilibrium data with higher R^2 values and lesser deviations. Thermodynamic studies reveal the exothermic ($\Delta H^o = -7.32$ kJ mol^{-1}) and spontaneous nature ($\Delta G^o = -7.78$ kJ mol^{-1}) of quinoline sorption onto MAW with increasing entropy of the system ($\Delta S^o = 1.52$ J K^{-1} mol^{-1}). The insight into the sorption mechanism shows the involvement of H-bonding, π–π dispersive interactions, boundary layer diffusion, and intraparticle diffusion in the sorption of quinoline. The

MW–chemically regenerated MAW shows quinoline sorption efficiency of 96.18, 94.71, and 92.68 % in three sorption–regeneration cycles as compared to ~97 % for virgin MAW. Approximately, 19.365 MJ of energy can be recovered per kg of quinoline-loaded sorbent, and the potential utilization of the bottom ash enhances the prospective of the candidate sorbent for wide-scale applications. The sorbent (MAW) has also been utilized by the authors for the adsorptive desulfurization of feed diesel and can also be exploited for the removal of heavy metals, dyes, and other toxic pollutants from aqueous and non-aqueous solutions. Thus, this study substantiates the utility of MAW for the remediation of pollutants for a clean and greener environment.

Acknowledgments Authors are grateful to the National Institute of Technology, Silchar, for providing laboratory facilities. Md. Juned K. Ahmed gratefully acknowledges the Ministry of Minority Affairs (MoMA), Government of India and University Grant Commission (UGC), New Delhi (F1-17.1/2012-13/MANF-2012-13-MUS-ASS-9763/(SA-III/Website)), for financial assistance under the Maulana Azad National Senior Research Fellowship (MANSRF).

References

Ahmaruzzaman M, Ahmed MJK, Begum S (2015) Remediation of Eriochrome black T-contaminated aqueous solutions utilizing H_3PO_4-modified berry leaves as a non-conventional adsorbent. Desalin Water Treat 56:1507–1519

Ahmed MJK, Ahmaruzzaman M (2015a) A facile synthesis of Fe_3O_4—charcoal composite for the sorption of a hazardous dye from aquatic environment. J Environ Manag 163:163–173

Ahmed MJK, Ahmaruzzaman M (2015b) Activated charcoal-magnetic nanocomposite for remediation of simulated dye polluted wastewater. Water Sci Technol 71:1361–1366

Ahmed MJK, Ahmaruzzaman M (2015c) Adsorptive desulfurization of feed diesel using chemically impregnated coconut coir waste. Int J Environ Sci Technol 12:2847–2856

Ahmed MJK, Ahmaruzzaman M (2015d) Fabrication and characterization of novel lignocellulosic biomass tailored Fe_3O_4 nanocomposites: influence of annealing temperature and chlorazol black E sequestration. RSC Adv 5:107466–107473

Ahmed MJK, Ahmaruzzaman M, Reza RA (2014) Lignocellulosic-derived modified agricultural waste: development, characterisation and implementation in sequestering pyridine from aqueous solutions. J Colloids Interface Sci 428:222–234

Ahmed MJK, Ahmaruzzaman M, Bordoloi MH (2015) Novel Averrhoa carambola extract stabilized magnetite nanoparticles: a green synthesis route for the removal of chlorazol black E from wastewater. RSC Adv 5:74645–74655

Ali I, Gupta VK (2007) Advances in water treatment by adsorption technology. Nat Protoc 1:2661–2667

Alonso-Davilla P, Torres-Rivera OL, Leyva-Ramos R, Ocampo-Perez R (2012) Removal of pyridine from aqueous solutions by adsorption on activated carbon cloth. CLEAN Soil Air Water 40:45–53

Ania CO, Parra JB, Menendez JA, Pis JJ (2005) Effect of microwave and conventional regeneration on the microporous and mesoporous network and on the adsorptive capacity of activated carbons. Microporous Mesoporous Mater 85:7–15

Baccar R, Blanquez P, Bouzid J, Feki M, Attiya H, Sarra M (2013) Modelling of adsorption isotherms and kinetics of a tannery dye onto an activated carbon prepared from an agricultural by-product. Fuel Proc Technol 106:408–415

Bai Y, Sun Q, Sun R, Wen D, Tang X (2011) Bioaugmentation and adsorption treatment of coking wastewater containing pyridine and quinoline using zeolite-biologically aerated filters. Environ Sci Techol 45:1940–1948

Burgos W, Nipon P, Mazzarese MC, Chorover J (2002) Adsorption of quinoline to kaolinite and montmorillonite. Environ Eng Sci 19:59–68

Collin G, Hoke H (1993) Quinoline and Isoquinoline. In: Elvers B, Hawkins S, Russey W, Schulz G (eds) Ullmann's encyclopaedia of industrial chemistry, A22. VCH, Weinheim, pp 465–469

Enriquez R, Pichat P (2001) Interactions of humic acid, quinoline, and TiO_2 in water in relation to quinoline photocatalytic removal. Langmuir 17:6132–6137

Freundlich HMF (1906) Over the adsorption in solution. Phys Chem 57:385–471

Gupta VK, Gupta B, Rastogi A, Agarwal S, Nayak A (2011) A comparative investigation on adsorption performances of mesoporous activated carbon prepared from waste rubber tire and activated carbon for a hazardous azo dye—Acid Blue 113. J Hazard Mater 186:891–901

Helfferich F (1963) Ion exchange. McGraw-Hill, New York

Jing J, Li W, Boyd A, Zhang Y, Colvin VL, Yu WW (2012) Photocatalytic degradation of quinoline in aqueous TiO_2 suspension. J Hazard Mater 237–238:247–255

Jing J, Li J, Feng J, Li W, Yu WW (2013) Photodegradation of quinoline in water over magnetically separable Fe_3O_4/TiO_2 photocatalyst. Chem Eng J 219:355–360

Jing J, Zhang Y, Li W, Yu WW (2014) Visible light driven photodegradation of quinoline over TiO_2/graphene oxide nanocomposites. J Catal 316:174–181

Kim D, Caruthers JM, Peppas NA (1993) Penetrant transport in crosslinked polystyrene. Macromolecules 26:1841–1847

Langmuir I (1916) The constitution and fundamental properties of solids and liquids. J Am Chem Soc 38:2221–2295

Liao P, Yuan S, Xie W, Zhang W, Tong M, Wang K (2013) Adsorption of nitrogen-heterocyclic compounds on bamboo charcoal: kinetics, thermodynamics, and microwave regeneration. J Colloid Interface Sci 390:189–195

Moon J, Dons KK, Won KL (1989) Adsorption equilibria for m-cresol, quinoline, and 1-naphthol onto silica gel. Korean J Chem Eng 6:172–178

Rameshraja D, Srivastava VC, Kushwaha JP, Mall ID (2012) Quinoline adsorption onto granular activated carbon and bagasse fly ash. Chem Eng J 181–182:343–351

Santhi T, Manonmani S, Smitha T, Mahalaxmi K (2009) Adsorption kinetics of cationic dyes from aqueous solution by bioadsorption onto activated carbon prepared from cucumis sativa. J Appl Sci Environ Sanit 4:263–271

Temkin MJ, Pyzhev V (1940) Kinetics of ammonia synthesis on prompted iron catalyst. Acta Physicochem URSS 12:217–256

Thomsen AB, Henriksen K, Gron C, Moldrup P (1999) Sorption, transport, and degradation of quinoline in unsaturated soil. Environ Sci Technol 33:2891–2898

Weber WJ, Morris JC (1962) Kinetics of adsorption of carbon from solution. J Sanit Eng Div Am Soc Civil Eng 89:31–59

Zhu S, Bell PRF, Greenfield PF (1988) Isotherm studies on sorption of pyridine and quinoline onto Rundle spent shale. Fuel 67:1316–1320